Using particle tracking to measure flow instabilities in an undergraduate laboratory experiment

Douglas H. Kelley and Nicholas T. Ouellette

Citation: American Journal of Physics **79**, 267 (2011); doi: 10.1119/1.3536647
View online: https://doi.org/10.1119/1.3536647
View Table of Contents: https://aapt.scitation.org/toc/ajp/79/3
Published by the American Association of Physics Teachers

Using particle tracking to measure flow instabilities in an undergraduate laboratory experiment

Douglas H. Kelley
Department of Mechanical Engineering and Materials Science, Yale University, New Haven, Connecticut 06520

Nicholas T. Ouellette[a)]
Department of Mechanical Engineering and Materials Science, Yale University, New Haven, Connecticut 06520

(Received 19 September 2010; accepted 7 December 2010)

Much of the drama and complexity of fluid flow occurs because its governing equations lack unique solutions. The observed behavior depends on the stability of the multitude of solutions, which can change with the experimental parameters. Instabilities cause sudden global shifts in behavior. We have developed a low-cost experiment to study a classical fluid instability. By using an electromagnetic technique, students drive Kolmogorov flow in a thin fluid layer and measure it quantitatively with a webcam. They extract positions and velocities from movies of the flow using Lagrangian particle tracking and compare their measurements to several theoretical predictions, including the effect of the drive current, the spatial structure of the flow, and the parameters at which instability occurs. The experiment can be tailored to undergraduates at any level or to graduate students by appropriate emphasis on the physical phenomena and the sophisticated mathematics that govern them.
[DOI: 10.1119/1.3536647]

I. INTRODUCTION

The striking and beautiful patterns formed by flowing fluids have fascinated scientists for millennia. From cloud dynamics[1] to climate change on Jupiter[2] to singular jets in a shaken dish,[3] fluid flow encompasses fascinating systems where complex phenomena can be clearly visualized, easily related to everyday life, and often explained qualitatively using simple arguments.

Central to understanding flow pattern formation is the concept of instability. Unlike most examples in undergraduate mathematics and physics courses, the differential equations that govern fluid motion have no unique solution. With more than one solution available, stability determines which will be observed. The same is true in mechanics, where the equations of motion of a pendulum allow it to be balanced upside-down, with its mass directly above its support. Any perturbation from that unstable position will cause it to fall and hang downward, and hence in everyday life we observe hanging pendulums far more often than inverted ones. In fluids, too, the less sensitive a given flow pattern is to perturbations, the more likely it is to be observed. A flow pattern that persists despite perturbations is called stable. As the flow parameters are varied, the pattern's sensitivity to perturbations may increase, leading to a sudden global transition in the flow. In that case, an *instability* is said to have occurred.

Many instabilities can be understood qualitatively by considering the competition between stabilizing and destabilizing effects. For example, in a quiescent fluid heated from below and cooled from above, the classic Rayleigh–Bénard instability[4] is a competition between the destabilizing effect of the temperature gradient and the stabilizing effects of viscous dissipation and thermal diffusion. When the tendency of the hot, buoyant bottom layer to rise exceeds the tendency of viscosity to retard motion or of thermal diffusion to conduct the excess heat away, the fluid will begin to flow. This type of competition can often be characterized by a dimensionless number (in this case, the Rayleigh number) which compares the two kinds of effects. When the number exceeds some critical value where the stabilizing effects are too weak, the system becomes unstable.

In this paper we describe a laboratory experiment suitable for undergraduates that allows not only visualization but also a quantitative study of a classic instability. Kolmogorov flow[5] was first proposed as a toy model for studying the transition to turbulence and is a two-dimensional series of parallel shear bands that becomes unstable and undergoes a transition to a vortex lattice when the destabilizing effects of shear win out over the stabilizing effect of viscosity. The flow can be generated in the laboratory with little effort or expense, and fits well in courses on fluid mechanics, nonlinear dynamics, classical mechanics, and in an advanced laboratory course. As a side benefit, the experiment also introduces students to present-day image processing and particle-tracking methods that are rapidly becoming measurement tools of choice in experimental fluid dynamics and related disciplines.[6]

We first present the basic theory underlying the instability to be measured. We then describe in detail the experimental setup (apparatus and measurement technique), discuss data obtained from the experiment, and compare to predictions where appropriate. Finally, we discuss the pedagogical aims of the experiment and suggest ways to integrate it into curricula at various levels.

II. THEORY

Like all physical systems, fluids obey conservation of momentum, which can be written as

$$\frac{\partial \boldsymbol{u}}{\partial t} + (\boldsymbol{u}\cdot\boldsymbol{\nabla})\boldsymbol{u} = -\frac{1}{\rho}\boldsymbol{\nabla} p + \nu\nabla^2\boldsymbol{u} + \boldsymbol{f}. \tag{1}$$

Here $\boldsymbol{u}$ is the velocity field, t is time, ρ is the (mass) density, p is the pressure field, ν is the kinematic viscosity, and $\boldsymbol{f}$

represents the applied body forces (per unit mass). The flow in the following experiments may be assumed to be incompressible because the speeds involved are much less than the speed of sound. Thus the flow satisfies the incompressibility condition

$$\boldsymbol{\nabla}\cdot\boldsymbol{u}=0. \tag{2}$$

Taken together, Eqs. (1) and (2) are known as the Navier–Stokes equations.

To eliminate the inconvenient pressure term, we can take the curl of Eq. (1), yielding

$$\frac{\partial\boldsymbol{\omega}}{\partial t}+(\boldsymbol{u}\cdot\boldsymbol{\nabla})\boldsymbol{\omega}-(\boldsymbol{\omega}\cdot\nabla)\boldsymbol{u}=\nu\nabla^2\boldsymbol{\omega}+\boldsymbol{F}, \tag{3}$$

where $\boldsymbol{\omega}=\boldsymbol{\nabla}\times\boldsymbol{u}$ is the vorticity and the last term $\boldsymbol{F}=\boldsymbol{\nabla}\times\boldsymbol{f}$ represents the forcing.

We will study Kolmogorov flow, that is, the flow that arises from the forcing

$$\boldsymbol{F}=F_0\sin\frac{2\pi x}{L}\hat{\boldsymbol{z}}. \tag{4}$$

A more accurate model of Kolmogorov flow in a container of finite depth would include a linear friction term to account for viscous drag at the bottom. Including the friction term turns out to be very important for making predictions of the experimental conditions at which instabilities occur, but changes little else,[7] and we will exclude it for simplicity.

Equations (2)–(4), together with appropriate boundary conditions, completely specify the behavior of the flow and admit multiple solutions. One very simple solution[5] is a series of steady stripes of alternating velocity (and correspondingly alternating vorticity), given by

$$\boldsymbol{u}_0=\sqrt{3}U\cos\frac{2\pi x}{L}\hat{\boldsymbol{y}}, \tag{5}$$

$$\boldsymbol{\omega}_0=\boldsymbol{\nabla}\times\boldsymbol{u}_0=-\sqrt{3}U\frac{2\pi}{L}\sin\frac{2\pi x}{L}\hat{\boldsymbol{z}}, \tag{6}$$

where $L/2$ is the stripe width and $U=\langle\boldsymbol{u}_0\cdot\boldsymbol{u}_0\rangle^{1/2}$ is the root-mean-square velocity. Substitution shows that the flow pattern given by Eq. (5) satisfies Eq. (3) provided that F_0 in Eq. (4) is $F_0=8\sqrt{3}\pi^3\nu UL^{-3}$. This solution is plotted in Fig. 1 and exists for all values of U, L, and ν.

Changing the flow parameters does not affect the existence of the solution $\boldsymbol{u}_0$, but does affect its stability. The stability of the flow is determined by the dimensionless combination of its parameters, $\mathrm{Re}=UL/\nu$, known as the Reynolds number. The Reynolds number expresses the relative importance of fluid inertia and viscous damping, and eliminates the need to consider U, L, and ν separately. It can be interpreted as the ratio of the time scale L^2/ν, characterizing viscous damping, to L/U, characterizing advection. If Re is small, viscous effects can damp perturbations, and $\boldsymbol{u}_0$ is the stable solution,[7] typically appearing first in experiments. As Re increases, a series of instabilities occur in which $\boldsymbol{u}_0$ gives way to a series of steady patterns, then traveling waves, and ultimately a set of period-doubling bifurcations that lead to chaos.[8] Students' opportunity to see this progression of instabilities is limited only by their experimental care (and perhaps the size of the power supply).

The first instability occurs when the stationary pattern of stripes $\boldsymbol{u}_0$ bifurcates to a stationary lattice of vortices. Their length scale, like that of $\boldsymbol{u}_0$, is set by the forcing scale L. Any instability causes qualitative changes to the flow pattern, but this instability is especially easy to identify visually because it corresponds to the onset of motion in the $\hat{\boldsymbol{x}}$ direction. Moreover, the instability occurs at modest Reynolds numbers easily accessible with a simple and inexpensive laboratory apparatus. This particular instability will be our focus for the rest of the paper. We sketch the linear stability analysis for this flow in the appendix.

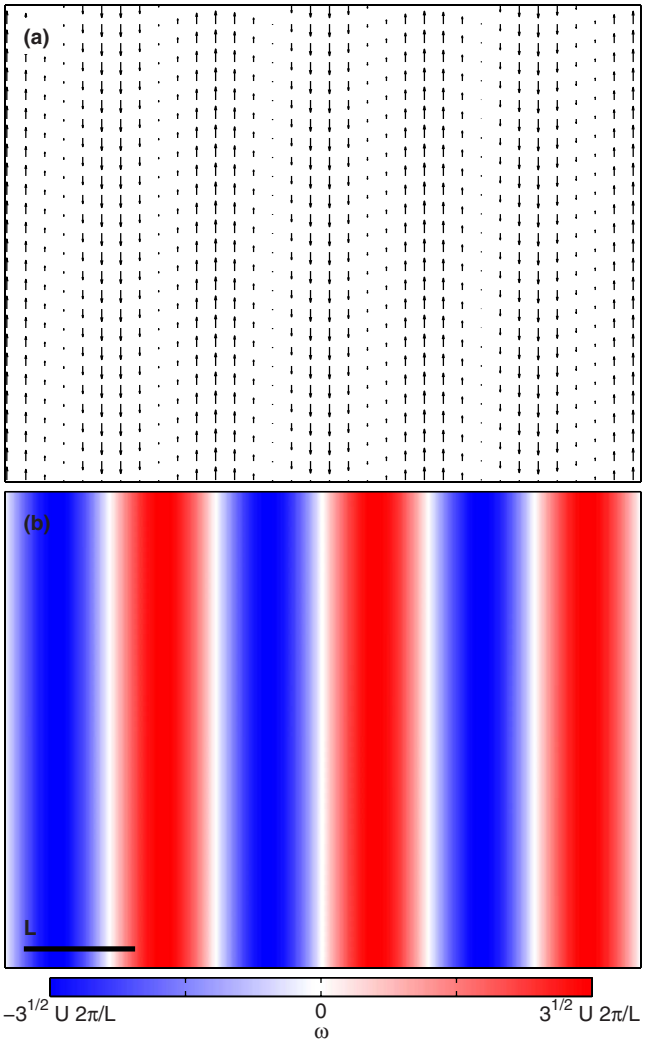

Fig. 1. The theoretical base flow $\boldsymbol{u}_0$. (a) Velocity field. (b) Vorticity field. The $\hat{\boldsymbol{x}}$ and $\hat{\boldsymbol{y}}$ directions are horizontal and vertical, respectively.

III. EXPERIMENTAL SETUP

Studying Kolmogorov flow in the laboratory requires an apparatus that can approximate two-dimensional motion by constraining flow to a plane as much as possible. The two most common systems for creating such quasi-two-dimensional flows in the laboratory are flowing soap films[9–12] and electromagnetically driven thin-layer flows.[13–18] We consider the latter class because they are simpler for students to set up. We place a shallow layer of an electrolyte, 5 mm deep and having lateral dimensions 248 mm $\times$286 mm, in an acrylic tray above an array of permanent magnets, as shown in Fig. 2. We used neodymium-iron-boron (NdFeB) grade N52 magnets, which produce a mag-

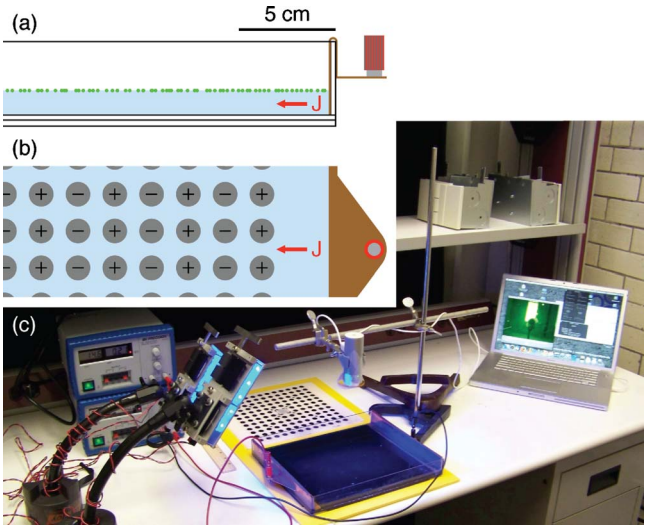

Fig. 2. The experimental apparatus. (a) Partial side view of the fluid layer and its tray. Tracer particles float at the fluid surface, and one electrode is visible at right. A current density $\boldsymbol{J}$ flows through the fluid. (b) Partial top view of an electrode and the magnet array. The polarity of each magnet is indicated by ± and the magnets are arranged in stripes perpendicular to $\boldsymbol{J}$. (c) The apparatus as assembled, with lamps, power supplies, camera, and the data acquisition computer. A second magnet array, arranged not for Kolmogorov flow but as an alternating square lattice (checkerboard), is also visible.

netic field of $\boldsymbol{B}\approx 0.3$ T at their surface. Each is 3.2 mm thick and 12.7 mm in diameter. They are placed in stripes of alternating polarity to approximate Kolmogorov flow according to Eq. (4). The stripe width $L/2$ of the flow $\boldsymbol{u}_0$ is set by the center-to-center spacing between the magnets, which is 19 mm. The array is a 12×12 square arrangement held in place by a perforated sheet of polyoxymethylene (Delrin). The fluid is a 10% by mass solution of $CuSO_4$ in water, mixed with glycerol (20% by volume) to increase the viscosity. The underside of the tray containing the test fluid is painted black for better imaging. A copper electrode is installed in each end of the fluid layer, and when a current I passes through the fluid, it causes a Lorentz force per unit mass

$$\boldsymbol{f}_B = \frac{\boldsymbol{J}\times\boldsymbol{B}}{\rho}, \tag{7}$$

where $\boldsymbol{J}$ is the current density, which produces bulk motion in the fluid. By using copper electrodes and a copper salt, we minimize unwanted electrochemical effects and precipitating reaction products. To produce the flows described below requires a power supply capable of 200 mA at 40 V.

The Reynolds number of the flow produced by an apparatus like this one can be estimated from dimensional arguments because the force per unit mass must scale as $f_B \sim U^2/L$.[19] We use Eq. (7) to estimate the current density as $J=NLI/V$, where V is the volume of fluid and NL is the distance between electrodes. We measured the magnetic field produced by an NdFeB magnet using an AlphaLab M1ST hand-held gaussmeter. The results are plotted in Fig. 3, showing $B=B_0e^{-z/\zeta}$ to a good approximation, where z is the axial distance from the center of the magnet face, $B_0=0.28$ T, and $\zeta=4.70$ mm. If we combine these estimates and measurements with the definition of Re and rearrange terms, we obtain

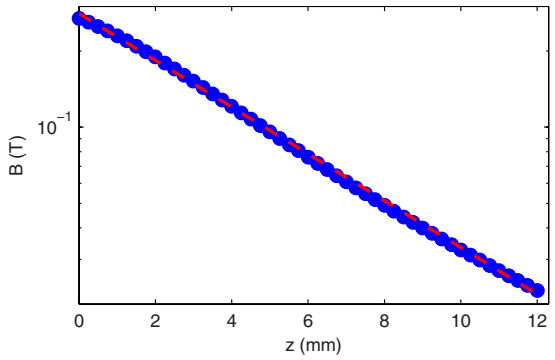

Fig. 3. Axial variation of the field of an example magnet. Circles show measurements made with a handheld gaussmeter. The dashed curve is an exponential fit $B=B_0e^{-z/\zeta}$ with $B_0=0.28$ T and $\zeta=4.70$ mm. The vertical scale is logarithmic.

$$\mathrm{Re} = \frac{CL^2}{\nu}\sqrt{\frac{NIB_0e^{-z/\zeta}}{\rho V}}, \tag{8}$$

where C is a dimensionless constant of order unity.

To visualize the motions that result from this sort of forcing, we add 80 μm fluorescent polystyrene spheres (ThermoFisher) to the fluid. With density 1.05 g/mL they are lighter than the electrolyte and float at its upper surface because buoyancy inhibits motion in the third dimension. Surface tension effects pose potential problems,[20] but can be minimized by keeping the seeding density low and adding a small amount of surfactant such as a drop of dish soap. The polystyrene spheres absorb most strongly in the blue (468 nm) and emit most strongly in the green (508 nm), making them well-suited for illumination by blue light emitting diodes. Blue LEDs typically have peak luminosity near 470 nm, and high-power versions (up to 50 lm each) are readily available and inexpensive. They can be powered with common DC laboratory power supplies. Figure 2 shows two banks of ten LEDs each, which are much brighter than necessary. Four LEDs, each positioned independently, might suffice to illuminate the experiments discussed here.

We recorded movies of the flowing particles with an Apple iSight webcam, which has an autofocus lens and records 30 frames per second, each 640 pixels wide and 480 pixels tall. Any webcam or digital camera capable of a similar frame rate and resolution could work as well, and a wide variety of inexpensive models are available. Manual control of the focus and gain would allow better scientific images. A frame rate that varies over time would make accurate measurements very difficult. To reduce glare, we attached a low-pass optical filter to the camera lens. The filter's 490 nm cutoff wavelength attenuates blue light from the LEDs substantially but allows green light from the particles to pass unaffected. Aligning the camera with the axis of the magnet array greatly simplifies the data analysis (see Fig. 7).

An apparatus to perform experiments like the one we have described can be constructed for around $250 and stocked with a large supply of tracer particles for about $250 more. Approximate costs appear in Table I. We have gathered the cleanest data when using very few particles so that a one gram vial would last years. The apparatus also produces visually compelling, but less quantitative, classroom demonstrations when seeded instead with a less expensive visualization fluid such as Kalliroscope.[21]

Table I. Approximate costs of the components of the experimental setup.

Part	Cost
Camera	$25
Optical filter	$30
4 LEDs with collimators	$40
Magnets	$80
Other construction materials	$75
Particles (1 g)	$250
Total	$500

Measurements can be made from movies of the flow by identifying and following tracer particles using Lagrangian particle tracking.[22] Specifically, we locate each particle in every frame by searching for local maxima of the brightness above some threshold, after the steady background image has been removed. We obtain the particle centers with a resolution of roughly 0.1 pixels (34 μm in the data described in the following) by fitting a one-dimensional Gaussian to the brightness field in each direction. With its location determined, each particle is matched to its location in other frames for as long as the particle can be followed. Our software makes these matches using a predictive three-frame best-estimate algorithm. For each partially constructed trajectory, the expected position of the particle at the next time step is estimated using simple kinematics. The measured particle position that comes closest to the estimate is chosen as a match, unless none is close enough. Small gaps in time are bridged with extrapolation. Gathering Lagrangian data is useful for many reasons.[23] In the experiments considered here, Lagrangian particle tracks conveniently allow a more accurate numerical differentiation scheme. We differentiate each trajectory in time by convolving with a Gaussian smoothing and differentiating kernel,[24] yielding a time series of positions and velocities for each tracked particle. Our post-processing Matlab software is freely available.[25]

In other work with higher-resolution cameras, we have routinely tracked as many as 30,000 particles per frame,[26] and an example of this sort of data is shown in Fig. 4. With a webcam we find that the instability can be more accurately quantified with just a few particles, say 100 per frame. Tracking particles requires tuning a set of parameters including the brightness threshold, the maximum frame-to-frame displacement of particles, and the number of predictive steps to perform. In a classroom setting, more or less of this tuning can be left to the students, depending on the scope of the experiment and the time allotted.

Fig. 4. Tracer particles in Kolmogorov flow, as seen from above. Fluorescent particles appear as bright dots in the original image; here the colors are inverted, so that particles are dark. Each follows local motions of the flowing fluid, as can be seen in the accompanying animation. It plays real-time and shows the response when a large (1.00 A) forcing current is applied to fluid at rest (Video 1 [URL: http://dx.doi.org/10.1119/1.3536647.1] enhanced online).

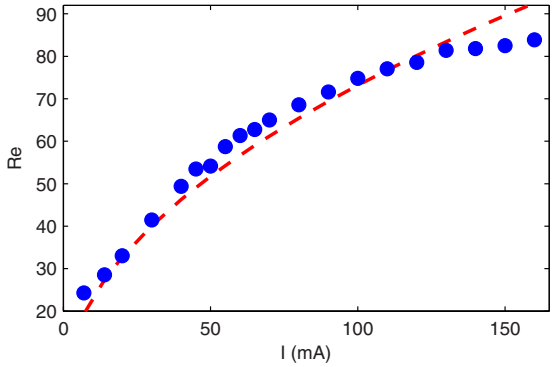

Fig. 5. Measured and predicted Reynolds number. Circles show the actual Reynolds number from root-mean-square velocities measured at 20 different currents. The dashed curve shows Re as predicted from dimensional arguments, using a least-squares fit to Eq. (8) which gives $C=0.42$.

The natural units of length and time of a digitized movie are pixels and frames, respectively. By recording an image of a ruler in place of the fluid, the pixel size can be easily determined and then used to convert pixel measurements to an SI length scale. Likewise, knowing the frame rate allows the use of an SI time scale.

IV. DATA ANALYSIS

Once particle trajectories have been constructed and differentiated, a wide variety of scientific questions can be addressed. It is possible to determine the Reynolds number for each value of the current I by determining the root-mean-square velocity $U=\langle \boldsymbol{u}\cdot\boldsymbol{u}\rangle^{1/2}$, where the measured velocity is $\boldsymbol{u}$ and the brackets $\langle\ \rangle$ signify averaging over all particles and all frames. Expressing Re this way is consistent with the notation of Eq. (5) when the flow $\boldsymbol{u}_0$ is present. The viscosity ν, also necessary for calculating the Reynolds number, can be measured using a variety of techniques. We used a capillary tube viscometer, simple enough for students and within the budget of most courses. From it we find the viscosity $\nu=2.61\times10^{-6}$ m^2 s^{-1}, which allows for the calculation of Re. The values of Re can be compared to the Reynolds number predicted by Eq. (8) after a few other laboratory measurements are made. We found $\rho=1.088$ g/mL, $z=8$ mm, $N=15$, and $V=350$ mL, then minimized the least-squared error between the measured and predicted values of Re to obtain the fit constant $C=0.42$; see Eq. (5). Its value varies with tracking parameters and other experimental details. Both the measured and predicted values of Re are shown in Fig. 5. The agreement is good considering the many approximations involved in the prediction, and serves as an example for students of the usefulness of estimation.

The spatial structure of the flow can also be investigated. In Fig. 6 we plot the measured vorticity in a subregion of the flow for Re=33, which confirms the theoretical prediction[5] that the stable flow at low Re is the pattern of stripes $\boldsymbol{u}_0$ shown in Fig. 1. We also plot the same subregion for Re

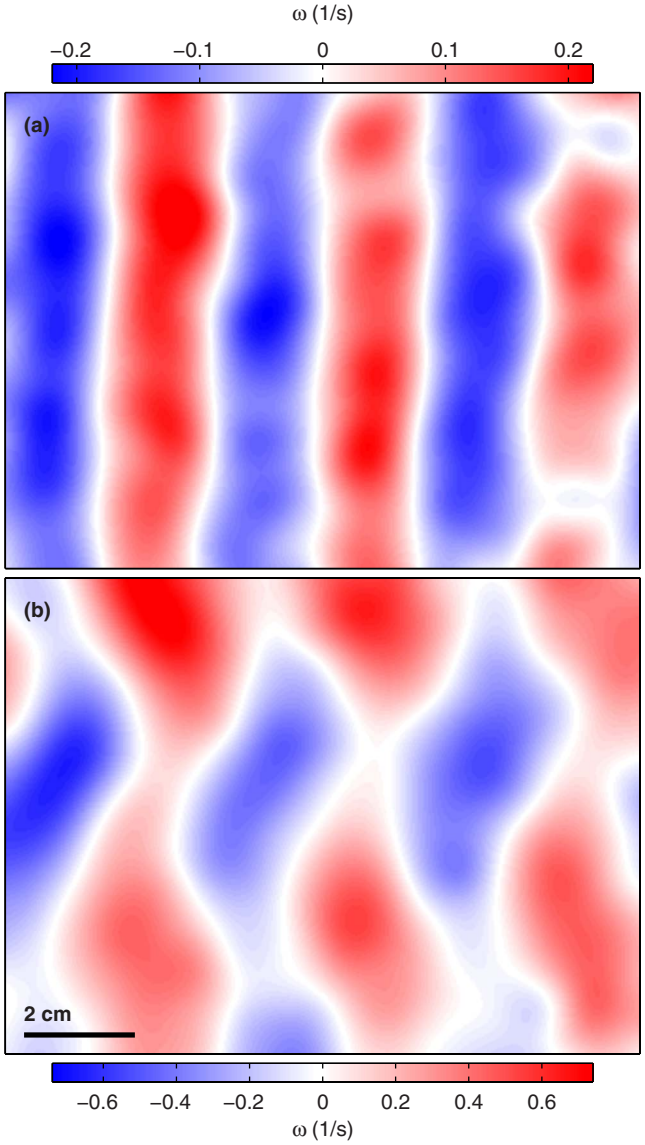

Fig. 6. Measured vorticity fields. (a) Measured base flow, with Re=33. (b) Measured flow at Re=72, after the first instability. Each field is a composite of 15 s of data. The $\hat{x}$ and $\hat{y}$ directions are horizontal and vertical, respectively.

=72, which confirms that as Re increases, an instability occurs in which stripes give way to an array of steady vortices. Both plots quantify the qualitative observations that can be made by eye.

We typically plot vorticity (the local angular velocity) instead of velocity because in a two-dimensional, incompressible flow, the scalar vorticity field uniquely and completely specifies the flow. Some extra effort is required because calculating the vorticity involves spatial gradients of the measured velocity field. Once the particle locations and velocities are known, a velocity field can be constructed via interpolation onto a regular grid. Spatial gradients can then be calculated by central differences or related schemes. Alternatively, the spatial gradients of particle velocities may be calculated at the (irregular) particle locations using techniques from finite element analysis. We used the Partial Differential Equation Toolbox in Matlab[27] to calculate vorticity in this way.

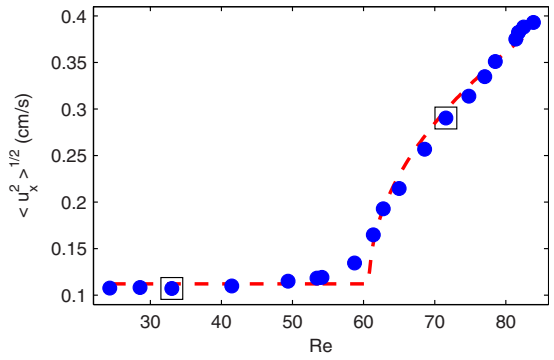

Fig. 7. Instability onset as a function of the measured Reynolds number. Circles show measured values of the root-mean-square velocity in the $\hat{x}$-direction. The dashed curve shows a prediction made by fitting the measurements to Eq. (9), yielding $A=0.6$ mm/s and $\mathrm{Re}_c=61$. Squares mark the data sets shown in Fig. 6.

From Fig. 6 it is clear that an instability occurs in the Kolmogorov flow in the range $33 \lesssim \mathrm{Re} \lesssim 72$. By tracking particles in movies recorded at several Reynolds numbers in this range, it is possible to locate the instability more accurately. Because the flow $\boldsymbol{u}_0$ involves no flow in the $\hat{\boldsymbol{x}}$ direction, this first instability can be found easily from the quantity $\langle u_x^2 \rangle^{1/2}$, where $u_x = \boldsymbol{u} \cdot \hat{\boldsymbol{x}}$. Figure 7 shows $\langle u_x^2 \rangle^{1/2}$ as a function of Re. Over the first seven data points, the overall flow speed (in terms of Re) more than doubles, while the $\hat{\boldsymbol{x}}$-direction flow (as measured by $\langle u_x^2 \rangle^{1/2}$) remains small and nearly constant. Its value in this range gives an estimate of the magnitude of the noise in our velocity measurements. As Re passes a critical value Re_c, $\langle u_x^2 \rangle^{1/2}$ increases suddenly and steadily in a manner characteristic of an instability.

The instability shown in Fig. 7 is a bifurcation of a steady solution ($\boldsymbol{u}_0$) which depends on a single control parameter (Re). The four simplest of such bifurcations, common in physical systems, are saddle-node, transcritical, pitchfork, and Hopf bifurcations.[28] Kolmogorov flow is governed by Eqs. (2)–(4), which have an analytic form different from the form of any of the four simplest cases. Predicting the precise shape of the bifurcation from first principles is beyond the scope of this paper. However, many bifurcations can be roughly matched to a square root near onset, and a crude model for the bifurcation observed here is

$$\langle u_x^2 \rangle^{1/2} = \begin{cases} u_{x0}, & \mathrm{Re} \le \mathrm{Re}_c \\ A\sqrt{\mathrm{Re} - \mathrm{Re}_c} + u_{x0}, & \mathrm{Re} > \mathrm{Re}_c. \end{cases} \tag{9}$$

For u_{x0} we use the mean value of the first seven data points plotted in Fig. 7. A least-squares fit to this model yields the dashed line also shown in Fig. 7, with $A=0.6$ mm/s. The instability occurs at the critical Reynolds number $\mathrm{Re}_c=61$. A previous study of Kolmogorov flow found a similar value, $\mathrm{Re}_c=70$.[12] The precise value of Re_c depends on the magnitude of the linear friction above and below the thin fluid layer,[7] a quantity difficult to measure.

V. PEDAGOGICAL AIMS AND CONTEXT

The experiment we have described introduces students to a number of scientific concepts. Foremost is the role of stability in governing the behavior of systems whose solutions are not unique, an idea nearly universal in fluid mechanics

but rarely addressed in undergraduate physics courses. The important quantity vorticity arises naturally as a straightforward parameter for addressing two-dimensional flow. If students have not previously encountered the Navier–Stokes equations, this experiment gives appropriate context and motivation for introducing them. A dimensional argument is useful to estimate the Reynolds number as a function of the forcing current, and the instability evident in Fig. 7 is a natural segue into bifurcation theory.

The experiment also offers students opportunity to develop a number of laboratory skills. They will adjust and measure the drive current to locate the instability. They will adjust lights and optics to produce clear images. In post-processing their data, they will convert movies to images, build a background image, and choose tracking parameters such as the minimum brightness threshold and maximum displacement between frames. Once the particles are tracked, students will construct plots like Figs. 6 and 7 from the raw velocity information, perhaps calculating spatial gradients themselves. They might also seek subsequent instabilities and make observations of the striking global rearrangements that occur at each onset.

We implemented this experiment over two weeks of a semester-long fluids laboratory course of mostly third- and fourth-year undergraduates. After a brief introduction, a single 3-h laboratory session was sufficient for groups of two or three students to mix the fluid, find the first instability, and record data. With one more hour they might also measure the viscosity of the fluid, as described. Another 3-h session was sufficient for tracking particles (using software that was provided and demonstrated) and performing the bulk of the analysis. An instructor was present for guidance throughout. Common mistakes included improper mixing of the test fluid, insufficient care in leveling the apparatus, using too many particles, and recording movies without first finding the instability. Depending on the intended scope, more or less assistance might be offered during post-processing. We have written software, available online, to simplify most steps, but much of the analysis (aside from the tracking itself) can be left entirely to the students. If time allows, students could also characterize the magnetic field.

Most of the concepts and skills that students will learn in this experiment fall outside the canon of common physics curricula and can be included at almost any level without redundancy. Upper-level undergraduates and beginning graduate students may have some familiarity with vector calculus and partial differential equations, but have probably been steered away from nonlinear equations such as the Navier–Stokes equations. Lower-level undergraduates might lack the mathematical background necessary to address the theory that underlies the experiment, but will gain intuitive understanding of instabilities nonetheless by seeing one with their own eyes. Because instabilities and bifurcation theory are rarely covered outside of courses in fluids or dynamical systems, this experiment could be used either to introduce those concepts or to complement those sorts of lecture courses. Particle tracking techniques will likely be new for all students and require no prerequisites. Students who expect to encounter fluids in the future—whether in medicine, science, or industry—have a good chance of benefiting from practical experience with particle tracking.

ACKNOWLEDGMENTS

We thank G. Weston-Murphy for building the flow cell. This work was partially supported by the U.S. National Science Foundation under Grant No. DMR-0906245.

APPENDIX: LINEAR STABILITY ANALYSIS

Here we sketch the linear stability analysis of the Kolmogorov flow, from which the critical Reynolds number of the primary instability can be calculated. The calculation changes slightly when the flow is bounded or a linear friction term is present in the governing equations,[7] but we give the stability analysis for the simplest case.

We begin with the vorticity Eq. (3)

$$\frac{\partial \boldsymbol{\omega}}{\partial t} + (\boldsymbol{u}\cdot\boldsymbol{\nabla})\boldsymbol{\omega} - (\boldsymbol{\omega}\cdot\boldsymbol{\nabla})\boldsymbol{u} = \nu\nabla^2\boldsymbol{\omega} + \hat{z}F_0 \sin kx, \tag{A1}$$

where the forcing is given by Eq. (4), $k=2\pi/L$ is the wavenumber of the forcing, and the incompressibility condition [Eq. (2)] applies: $\boldsymbol{\nabla}\cdot\boldsymbol{u}=0$. As with any two-dimensional incompressible flow problem, it is convenient to work in terms of the streamfunction ψ, defined so that

$$u_x = \frac{\partial \psi}{\partial y} \tag{A2}$$

and

$$u_y = -\frac{\partial \psi}{\partial x}. \tag{A3}$$

We note that ψ plays the role of a Hamiltonian. In two dimensions the vorticity is a scalar (or, equivalently, is a vector that is constrained to point normal to the plane) given by $\omega=-\nabla^2\psi$. We substitute this definition into Eq. (A1) and obtain

$$\frac{\partial}{\partial t}\nabla^2\psi + \frac{\partial \psi}{\partial y}\frac{\partial}{\partial x}\nabla^2\psi - \frac{\partial \psi}{\partial x}\frac{\partial}{\partial y}\nabla^2\psi = \nu\nabla^2\nabla^2\psi - F_0 \sin kx. \tag{A4}$$

As can be checked by taking derivatives, the base Kolmogorov flow [Eq. (5)] is given by the stream function

$$\psi_0 = -\frac{\sqrt{3}U}{k}\sin kx. \tag{A5}$$

We now introduce an infinitesimal perturbation $\tilde{\psi}$ so that the total streamfunction is given by $\psi=\psi_0+\tilde{\psi}$. Our goal is to determine whether this perturbation grows or decays. We insert this form of ψ into Eq. (A4) and linearize it in $\tilde{\psi}$, dropping terms of order $\tilde{\psi}^2$ or higher, because the perturbation is assumed to be infinitesimal. Because ψ_0 satisfies Eq. (3), we have

$$\frac{\partial}{\partial t}\nabla^2\tilde{\psi} + \frac{\partial \psi_0}{\partial y}\frac{\partial}{\partial x}\nabla^2\tilde{\psi} + \frac{\partial \tilde{\psi}}{\partial y}\frac{\partial}{\partial x}\nabla^2\psi_0 - \frac{\partial \psi_0}{\partial x}\frac{\partial}{\partial y}\nabla^2\tilde{\psi} - \frac{\partial \tilde{\psi}}{\partial x}\frac{\partial}{\partial y}\nabla^2\psi_0 = \nu\nabla^2\nabla^2\tilde{\psi}. \tag{A6}$$

If we use the explicit form for ψ_0 in Eq. (A2) and express lengths and velocities in terms of $L=2\pi/k$ and by U respectively, we can write Eq. (A6) as

$$\frac{\partial}{\partial t}\nabla^2\tilde{\psi} + \sqrt{3}\cos 2\pi x(\nabla^2 + 4\pi^2)\frac{\partial\tilde{\psi}}{\partial y} = \frac{\sqrt{3}}{\mathrm{Re}}\nabla^2\nabla^2\tilde{\psi}. \quad \text{(A7)}$$

Following the usual prescriptions in linear stability theory,[29,30] we expand the perturbation $\tilde{\psi}$ in normal modes. Because the equation of motion for $\tilde{\psi}$ is linear in time, we assume a time dependence of the form $e^{\sigma t}$, where σ is the growth rate of the perturbation. Because the flow is unbounded and uniform in the y direction, we represent the y dependence of $\tilde{\psi}$ by a Fourier mode of wavenumber q, so that we can account for a perturbation of arbitrary scale. The x dependence is more difficult to treat. We assume that the x dependence is given by some function $f(x)$. We therefore have

$$\tilde{\psi}(t,x,y) = e^{\sigma t}e^{iqy}f(x). \quad \text{(A8)}$$

If we substitute this form into Eq. (A7) and simplify, we arrive at

$$\sigma\left(\frac{\partial^2}{\partial x^2} - q^2\right)f + iq\sqrt{3}\cos 2\pi x\left(\frac{\partial^2}{\partial x^2} - q^2 - 4\pi^2\right)f = \frac{\sqrt{3}}{\mathrm{Re}}\left(\frac{\partial^2}{\partial x^2} - q^2\right)^2 f. \quad \text{(A9)}$$

This ordinary differential equation in x is a form of the Orr–Sommerfeld equation,[30] and can be interpreted as an eigenvalue problem for the growth rate σ and the associated eigenfunction f. For a given combination of Re, q, and f, Eq. (A9) can be used to determine the stability of the system. If $\sigma<0$, the perturbation decays and the base flow $\boldsymbol{u}_0$ is stable, and if $\sigma>0$, the perturbation grows and the flow $\boldsymbol{u}_0$ is unstable.

[a]Electronic mail: nicholas.ouellette@yale.edu

[1]R. A. Shaw, "Particle-turbulence interactions in atmospheric clouds," Annu. Rev. Fluid Mech. **35**, 183–227 (2003).
[2]P. S. Marcus, "Prediction of a global climate change on Jupiter," Nature (London) **428**, 828–831 (2004).
[3]B. W. Zeff, B. Kleber, J. Fineberg, and D. P. Lathrop, "Singularity dynamics in curvature collapse and jet eruption on a fluid surface," Nature (London) **403**, 401–404 (2000).
[4]E. Bodenschatz, W. Pesch, and G. Ahlers, "Recent developments in Rayleigh-Bénard convection," Annu. Rev. Fluid Mech. **32**, 709–778 (2000).
[5]A. M. Obukhov, "Kolmogorov flow and laboratory simulation of it," Russ. Math. Surveys **38**, 113–126 (1983).
[6]N. T. Ouellette, in *Experimental and Computational Techniques in Soft Condensed Matter Physics*, edited by J. Olafsen (Cambridge U. P., Cambridge, 2010).
[7]A. Thess, "Instabilities in two-dimensional spatially periodic flows. Part I: Kolmogorov flow," Phys. Fluids A **4**, 1385–1395 (1992).
[8]F. Feudel and N. Seehafer, "Bifurcations and pattern formation in a two-dimensional Navier-Stokes fluid," Phys. Rev. E **52** (4), 3506–3511 (1995).
[9]Y. Couder, "Two-dimensional grid turbulence in a thin liquid film," J. Physique Lett. **45**, 353–360 (1984).
[10]H. Kellay, X.-L. Wu, and W. I. Goldburg, "Experiments with turbulent soap films," Phys. Rev. Lett. **74**, 3975–3978 (1995).
[11]P. Vorobieff and R. E. Ecke, "Fluid instabilities and wakes in a soap-film tunnel," Am. J. Phys. **67**, 394–399 (1999).
[12]J. M. Burgess, C. Bizon, W. D. McCormick, J. B. Swift, and H. L. Swinney, "Instability of the Kolmogorov flow in a soap film," Phys. Rev. E **60** (1), 715–721 (1999).
[13]P. Tabeling, S. Burkhart, O. Cardoso, and H. Willaime, "Experimental study of freely decaying two-dimensional turbulence," Phys. Rev. Lett. **67**, 3772–3775 (1991).
[14]D. Rothstein, E. Henry, and J. P. Gollub, "Persistent patterns in transient chaotic fluid mixing," Nature (London) **401**, 770–772 (1999).
[15]T. H. Solomon and I. Mezić, "Uniform resonant chaotic mixing in fluid flows," Nature (London) **425**, 376–380 (2003).
[16]H. J. H. Clercx, G. J. F. van Heijst, and M. L. Zoeteweij, "Quasi-two-dimensional turbulence in shallow fluid layers: The role of bottom friction and fluid layer depth," Phys. Rev. E **67**, 066303 (2003).
[17]M. K. Rivera and R. E. Ecke, "Pair dispersion and doubling time statistics in two-dimensional turbulence," Phys. Rev. Lett. **95**, 194503 (2005).
[18]L. Rossi, J. C. Vassilicos, and Y. Hardalupas, "Electromagnetically controlled multi-scale flows," J. Fluid Mech. **558**, 207–242 (2006).
[19]N. F. Bondarenko, M. Z. Gak, and F. V. Dolzhanskii, "Laboratory and theoretical models of plane periodic flow," Akademiia Nauk SSSR Fizika Atmosfery i Okeana **15** (1), 1017–1026 (1979).
[20]D. Vella and L. Mahadevan, "The 'Cheerios effect'," Am. J. Phys. **73**, 817–825 (2005).
[21]Kalliroscope Corporation, ⟨www.kalliroscope.com/⟩.
[22]N. T. Ouellette, H. Xu, and E. Bodenschatz, "A quantitative study of three-dimensional Lagrangian particle tracking algorithms," Exp. Fluids **40**, 301–313 (2006).
[23]F. Toschi and E. Bodenschatz, "Lagrangian properties of particles in turbulence," Annu. Rev. Fluid Mech. **41**, 375–404 (2009).
[24]N. Mordant, E. Lévêque, and J. F. Pinton, "Experimental and numerical study of the Lagrangian dynamics of high Reynolds turbulence," New J. Phys. **6**, 116 (2004).
[25]See supplementary material at http://dx.doi.org/10.1119/1.3536647 for the post-processing software. This document can also be downloaded at ⟨leviathan.eng.yale.edu⟩.
[26]S. T. Merrifield, D. H. Kelley, and N. T. Ouellette, "Scale-dependent statistical geometry in two-dimensional flow," Phys. Rev. Lett. **104**, 254501 (2010).
[27]Matlab is published by MathWorks ⟨www.mathworks.com/⟩.
[28]M. C. Cross and P. C. Hohenberg, "Pattern formation outside of equilibrium," Rev. Mod. Phys. **65** (3), 851–1112 (1993).
[29]S. Chandrasekhar, *Hydrodynamic and Hydromagnetic Stability* (Dover, New York, 1961).
[30]P. G. Drazin and W. H. Reid, *Hydrodynamic Stability*, 2nd ed. (Cambridge U. P., Cambridge, 2004).